Construction and Building Materials 173 (2018) 28–39

Contents lists available at ScienceDirect

Construction and Building Materials

journal homepage: www.elsevier.com/locate/conbuildmat

Physical and mechanical properties of fly ash and slag geopolymer concrete containing different types of micro-encapsulated phase change materials

Shima Pilehvar [a,b], Vinh Duy Cao [a,c], Anna M. Szczotok [a,d], Manuel Carmona [d], Luca Valentini [e], Marcos Lanzón [f], Ramón Pamies [b], Anna-Lena Kjøniksen [a,*]

[a] Faculty of Engineering, Østfold University College, P.O. Box 700, 1757 Halden, Norway
[b] Department of Materials Engineering and Manufacturing, Technical University of Cartagena, Cartagena, Murcia, Spain
[c] Department of Mathematical Science and Technology, Norwegian University of Life Science, N-1432 Ås, Norway
[d] Department of Chemical Engineering, University of Castilla – La Mancha, 13004 Ciudad Real, Spain
[e] Department of Geosciences, University of Padua, 35131 Padua, Italy
[f] Departamento de Arquitectura y Tecnología de la Edificación, Escuela Técnica Superior de Arquitectura e Ingeniería de Edificación ETSAE, Universidad Politécnica de Cartagena, 30203 Alfonso XIII 52, Cartagena, Spain

HIGHLIGHTS

- High compressive strength of fly ash/slag geopolymer concrete containing microcapsules.
- Effect of different types of micro-encapsulated phase change materials.
- Microcapsules change the workability of geopolymer concrete.
- Microcapsule addition affects the setting time of geopolymer paste.
- Shell type and agglomeration of microcapsules strongly influence the concrete properties.

GRAPHICAL ABSTRACT

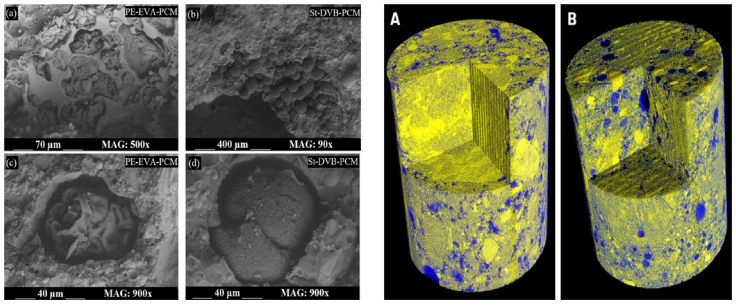

ARTICLE INFO

Article history:
Received 7 November 2017
Received in revised form 1 April 2018
Accepted 2 April 2018

Keywords:
Geopolymer concrete
Mix design
Micro-encapsulated phase change materials
Compressive strength
Microstructure

ABSTRACT

A mix design procedure for geopolymer concrete (GPC) was developed in order to maintain a high compressive strength after adding micro-encapsulated phase change materials (MPCM). The most relevant factors which affect the properties of fly ash/slag based GPC containing MPCM are considered. Class F fly ash and slag, sodium hydroxide and sodium silicates were chosen as binder and alkaline solution, respectively. Two types of MPCM were used for a better understanding the effect of different MPCMs on the properties of the GPC. The setting time of geopolymer pastes was found to depend on both the amount of water adsorbed by the microcapsules, the viscosities of the samples, and possibly the latent heat. Accordingly, the initial setting time increased and the final setting time decreased with MPCM concentration. A slump test and compressive strength measurements have been utilized to examine the workability and mechanical properties of the new mix design. It was observed that the addition of MPCM reduces the slump and the compressive strength of GPC. These effects were more pronounced for the MPCM that form agglomerated structures and has a surface containing some polar groups, than for the more spherically shaped and less agglomerated MPCM with a hydrophobic surface. Although the addition of MPCM reduced the compressive strength of geopolymer concrete, the mechanical performance was higher than that of Portland cement concrete after 28 days of curing. A combination of SEM imaging and X-ray-tomography suggested that MPCM agglomeration, gaps between MPCM and the

* Corresponding author.
E-mail address: anna.l.kjoniksen@hiof.no (A.-L. Kjøniksen).

https://doi.org/10.1016/j.conbuildmat.2018.04.016
0950-0618/

concrete matrix, an increased amount of entrapped air, and microcapsules that break under stress might contribute to the reduced compressive strength of GPC.

1. Introduction

The demand for cementitious materials has increased considerably in recent years. Ordinary Portland cement is normally considered as the main material for construction purposes. However, the Portland cement production has a severe impact on the environment due to the huge amount of greenhouse gases emitted to the atmosphere [1,2]. In the early 80 s geopolymers were introduced as alternative construction materials with a lower environmental impact [3]. The geopolymer binder is synthesized by mixing materials rich in silica and amorphous alumina with a strong alkaline activator [4]. Geopolymers are a very interesting concrete alternative, with an improved performance compared to traditional concretes [5], while utilizing a high proportion of industrial by-products such as fly ash (FA), coal ash and blast furnace slag.

The incorporation of micro-encapsulated phase change materials (MPCM) in building materials, such as mortar and concrete can improve the thermal energy storage capacity of building structures, thereby decreasing the energy demand in buildings [6]. However, the presence of MPCM decreases the workability and mechanical strength of concrete [7]. In spite of reducing the concrete compressive strength by addition of MPCM, it is still often high enough to be used in building constructions.

When developing geopolymer concrete (GPC) formulations, the type, amount and ratio of the raw materials, curing time and temperature needs to be taken into account [4]. Several previous studies discuss the mix design of GPC considering the workability and strength [8,9]. However, few studies consider the properties of geopolymer compositions with incorporated MPCM [7,10]. The objective of this paper is designing a GPC mixture with improved mechanical properties and better workability, to compensate for the negative effect of incorporated MPCM on these properties. An accurate and convenient mix design method for fly ash/slag geopolymer concrete with incorporated MPCM has been developed. Since different types of MPCM may influence the GPC in different ways, two kinds of MPCMs were compared.

2. Background

In order to formulate a good GPC mix-design, it is important to know how different factors will affect the properties of fly ash/slag based GPC.

2.1. Aluminosilicate

Fly ash (FA) is considered to be one of the main sources of silica (SiO_2) and alumina (Al_2O_3) in GPC. In accordance with ASTM C618, FA is classified based on its chemical composition, where the main difference is the calcium amount. FA class C has a higher content of calcium than FA class F. A higher content of CaO in the FA results in a higher compressive strength of GPC due to the formation of hydrated products, such as calcium silicate hydrate (CSH) [11]. However, at these conditions the setting time of GPC decreases noticeably (less than 3 min) [11]. Fly ash class F has therefore been selected as a good raw material for GPC due to the lower reactivity rate, which leads to a slower setting time, convenient accessibility, and a reduced water demand [12]. In order to improve the mechanical properties of class F fly ash GPC, small amounts of other additives which are rich in CaO (e.g., blast furnace slag, silica fume, or natural pozzolan) can be added [12,13]. Ground granulated blast furnace slag (GGBFS) is one of the most common components in geopolymer mortar and concrete, due to improved mechanical and microstructural properties [12]. However, adding GGBFS causes poor workability due to a higher viscosity [14]. Chemical admixtures can be used to improve the workability of GPC.

2.2. Alkaline solution

The alkaline solution dissolves Al^{3+} and Si^{4+} ions from the aluminosilicate sources, which subsequently improves compressive strength by forming sodium aluminosilicate hydrate (NASH), calcium alumino silicate (CASH), and/or calcium silicate hydrate (CSH) gels [15]. The most common alkaline solutions are sodium hydroxide (NaOH), potassium hydroxide (KOH), sodium silicate (Na_2SiO_3) and potassium silicate (K_2SiO_3). The dissolution of fly ash and slag is dependent on the type and concentration of the alkaline solution [16]. Utilizing a sodium hydroxide alkaline solution as an alkaline activator in GPC is found to be more effective than a potassium hydroxide solution, since NaOH(aq) dissolves a higher amount of Al^{3+} and Si^{4+} ions than KOH(aq) [17]. In addition, the concentration of the alkaline solution influences the workability and compressive strength of GPC, and an optimum value of 16 M NaOH has been reported for some systems [18]. Using a combination of sodium hydroxide and sodium silicate results in a higher compressive strength than when only sodium hydroxide is used [15] due to formation of a higher amount of calcium silicate hydrate (CSH) when sodium silicate is used [15]. The ratio of sodium silicate to sodium hydroxide is important [18], since the high viscosity of sodium silicate in the alkaline solution reduces the slump of GPC in comparison with Portland cement concrete [7].

2.3. Micro-encapsulated phase change materials

The workability of concrete decreases in the presence of MPCM. This might be due to differences in the particle size of MPCM compared with the sand it replaces, or due to a reduction of available water in the sample caused by the water affinity of the MPCM shell [19]. Another possible drawback of MPCM addition to mortar or concrete is a reduction of the compressive strength [6,7,10]. However, the compressive strength is still sufficiently high for structural applications, since the acceptable range of compressive strength for building structures is normally within 25–40 MPa.

2.4. Extra water and chemical admixture

Fresh GPC possesses poor workability in comparison with fresh Portland cement concrete due to the higher viscosity of the alkaline solution. Both the workability and compressive strength of GPC are negatively influenced by the incorporation of MPCM. A better workability can be obtained by adding extra water to the mixture. However, this will reduce the compressive strength of GPC [18]. A better solution is therefore to utilize a chemical admixture. Naphthalene based superplasticizers improve the workability of fly ash class F mixtures [20]. A polycarboxylate-based superplasticizer is often the best choice for fly ash class C, due to the strong

bonds between the positively charged calcium and the negatively charged polycarboxylate [20].

3. Experimental

3.1. Materials

The class F FA (density = 2.26 ± 0.02 g/cm^3) was purchased from Norcem, Germany and GGBFS (density = 2.85 ± 0.02 g/cm^3) was supplied by Cemex, Germany. The chemical composition of fly ash and GGBFS determined by X-ray Fluorescence (XRF) is given in Table 1.

Sodium hydroxide pellets (density = 2.13 g/cm^3) and sodium silicate solution (density = 1.93 g/cm^3, 35 wt% solid) purchased from VWR, Norway, were used for preparation of the alkaline solution. FLUBE OS 39 (density of 1.20 g/cm^3), a poly-naphthalene sulfonate polymer from Bozzetto Group, Italy, was used as a superplasticizing admixture to improve the workability of GPC and decrease the amount of extra water. This superplasticizer was chosen due to the good effect of naphthalene based superplasticizers on the workability geopolymer concrete containing fly ash class F [20].

Both sand (density of 2.68 g/cm^3) and gravel (density of 2.62 g/cm^3) were provided by Gunnar Holth and Skolt Pukkverk AS, originating from Mysen and Råde, Norway.

In order to reduce the effect of the water affinity of the MPCM shell, two MPCMs with hydrophobic shells were utilized. The core material for both MPCMs is a paraffin wax (Rubitherm®RT27), but the shell for the first MPCM is a copolymer consisting of low density polyethylene (LDPE) and ethylvinylacetate (EVA) and the second MPCM has a copolymer shell of styrene (St) and divinylbenzene (DVB) [21,22]. These microcapsules are named PE-EVA-PCM and St-DVB-PCM, respectively. The general properties of PE-EVA-PCM and St-DVB-PCM are presented in Table 2.

SEM images of PE-EVA-PCM and St-DVB-PCM are provided in Fig. 1 to illustrate the differences in shape and size. As can be seen from Fig. 1a, the individual particles of PE-EVA-PCM have an uneven shape and are agglomerated into clusters with an irregular structure, while St-DVB-PCM (Fig. 1b) is present as single, unagglomerated spherical particles. In addition, St-DVB-PCM seems to have a narrower size distribution than PE-EVA-PCM.

Table 1
Chemical composition of fly ash (FA) and ground granulated blast furnace slag (GGBFS).

Chemical	FA (wt%)	GGBFS (wt%)
Al_2O_3	23.15	10.30
SiO_2	50.83	34.51
CaO	6.87	42.84
Fe_2O_3	6.82	0.60
MgO	1.70	7.41
K_2O	2.14	0.52
TiO_2	1.01	0.67
Na_2O	1.29	0.4
P_2O_5	1.14	0.02
SO_3	1.24	1.95
SrO	0.19	0.05
CO_2	3.07	0.30

Table 2
Properties of PE-EVA-PCM and St-DVB-PCM [21,22].

General properties	PE-EVA-PCM	St-DVB-PCM
Form	Non-spherical	Spherical
Synthesizing technique	Spray drying	Suspension-like polymerization
Shell composition	Low density polyethylene (50 wt%) Ethylvinylacetate (50 wt%)	Styrene (50 wt%) Divinylbenzene (50 wt%)
Core material	Paraffin	Paraffin
Melting point	28.4 ± 0.9 °C	24.2 ± 0.9 °C
Specific gravity	0.9 g/cm^3	0.9 g/cm^3
Latent heat	98.1 J/g	96.1 J/g

3.2. Experimental methods

3.2.1. Particle size distribution and moisture content

The particle size distribution analysis of sand and gravel was carried out by mechanical sieving according to EN 933-1. The particle size distribution of FA, GGBFS, and MPCMs were determined by Low Angle Laser Light Scattering laser diffraction (Malvern Mastersizer 2000). The moisture content and trapped water of MPCMs and sand were calculated by a moisture analyser (MB series, VWR). The materials were dried at 50 °C until the mass loss was less than 5%, before immersing in water for 1 day. Afterward, the materials were sieved (mesh size of 250 μm) for 2 min and transferred to the moisture analyzer. In order to prevent the decomposition of the MPCM shell, the water adsorbed and retained by the materials were measured at 50 °C.

3.2.2. Setting time

The initial and final setting times of geopolymer paste containing 0, 10, and 20% of PE-EVA-PCM or St-DVB-PCM were performed with a computer controlled Vicat needle instrument (ToniSET One, Model 7301) in accordance with EN 196-3. The initial setting time was calculated from when the mixing of raw materials was initiated, and continued up to the final setting time with an interval of 2 min. The setting time measurement was carried out at 20 °C.

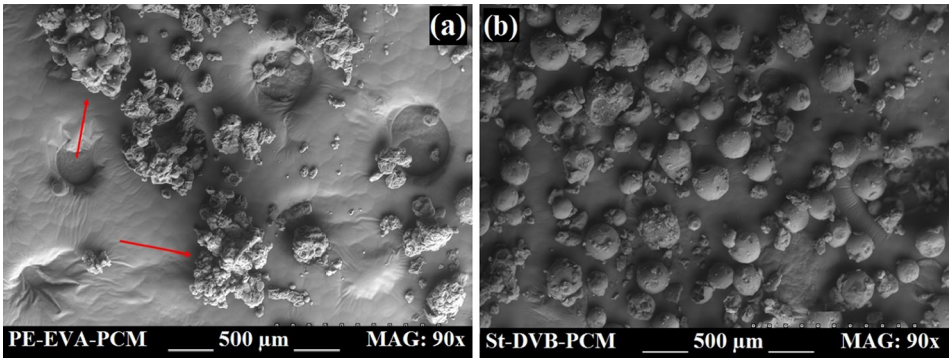

Fig. 1. SEM images of (a) PE-EVA-PCM (b) St-DVB-PCM. The arrows in (a) show the agglomerated structures of PE-EVA-PC.

3.2.3. Slump flow test

The workability of fresh GPC where 0, 10 and 20% of the sand was replaced by PE-EVA-PCM or St-DVB-PCM was measured immediately after mixing by a slump test in accordance with EN 12350-2. An Abrams cone was used as the mold. The cone dimensions were 300 mm in height, and 100 mm and 200 mm in diameters at the top and base, respectively.

3.2.4. Compressive strength test

The compressive strength tests were carried out in accordance with EN 12390–3. In this study, the compressive strength was determined using digital compressive strength test machine (Form + Test Machine) with a load cell capacity of 3000 kN. Each test cube was exposed to a force at a loading rate of 0.8 kN/s until it failed. The compressive strength tests were performed at 20 °C on GPC specimens where 0, 10 and 20 vol% of the sand was replaced by PE-EVA-PCM or St-DVB-PCM at curing times of 1, 7, 14, and 28 days. For each compression test, three cubes were left in the room for 1 h (to remove free water from the surfaces), then weighed and tested. The reported values are the average of the three cubes.

3.2.5. Scanning electron microscopy (SEM) imaging

The microstructure of the fractured surfaces of GPC containing 0 and 20% of PE-EVA-PCM and St-DVB-PCM was analyzed using Hitachi S3500N Scanning Electron Microscope (SEM) at an accelerating voltage of 15 kV. The images were captured in BSE (back scattered electrons) mode to obtain adequate contrast between lightweight materials (PCM) and the cementitious matrix (geopolymer).

3.2.6. X-ray microtomography

X-ray microtomography (XCT) scans were performed on cylinders with a diameter of 1 cm, drilled from the GPC samples utilizing a Skyscan 1172 (Bruker, Billerica, US). The samples were irradiated by W radiation with 80 kV source voltage and 0.7 s exposure time over a 180° rotation with 0.3° angular steps. Cross-sectional slices were obtained by tomographic reconstruction using the Feldkamp algorithm [23]. 3D rendering was performed by the Bruker CTVox software on subvolumes consisting of 1000 stacked circular slices with 1000 pixel diameter (6 μm pixel size). Conversion to binary images was achieved using an iterative thresholding algorithm [24]. The negligible X-ray absorption of low atomic number elements present in MPCM, facilitated the segmentation process of the 7 images that were easily converted into the binary images.

3.2.7. Energy saving

To investigate the effect of microcapsules on the energy saving performance of the geopolymer concrete, a small test box was utilized. The text box was made from 50 mm polyethylene expanded foam (PEF) panels. The concrete sample (200 × 200 × 50 mm) was inserted in a matching opening in the box. The test box was placed inside an environmental chamber to mimic the outdoor environmental temperature variations. The simulated indoor temperature (T_{room}) was set at 23 °C throughout the experiment using a Laird temperature regulator (AA150-Laird Technologies). To mimic outdoor conditions, the outdoor temperature T_{out} was imposed as a sinusoidal function of time using an environmental chamber (VT^3 4250, Vötsch, Germany):

$$T_{out}(t) = \frac{T_{max} + T_{min}}{2} + \frac{T_{max} - T_{min}}{2} \sin\left(\frac{\pi}{43200} t - \frac{2\pi}{3}\right) \quad (1)$$

where T_{max} = 40 °C and T_{min} = 10 °C are the maximum and minimum outdoor temperatures during a day, respectively. Outdoor temperature cycles (Eq. (1)) were run for 72 h, starting at a steady state of 23 °C.

The temperature and heat fluxes on both surfaces of the sample were recorded by using thermocouples and heat flux sensors to measure heat losses towards the simulated indoor environment. The total energy supplied to the heating/cooling system to maintain the simulated indoor temperature at 23 °C within one day can be calculated as the sum of the heating and cooling power consumption:

$$P = \frac{\int_{t_{ini}}^{t_{end}} |\varphi_{indoor}| dt}{3600 \cdot 10^3} \quad (2)$$

where φ_{indoor} is the heat flux on the simulated indoor side of the sample, t_{ini} and t_{end} are the initial time and end time of the thermal cycle. The power reduction Pr was calculated from:

$$Pr = \frac{P_{GPC} - P_{MPCM-GPC}}{P_{GPC}} \cdot 100\% \quad (3)$$

where P_{GPC} and $P_{MPCM\text{-}GPC}$ are the 24 h power consumption of the heating and cooling system for geopolymer concrete without MPCM and with MPCM, respectively. For more details regarding the experimental setup, see Cao et al. [25].

4. Mix design procedure

The geopolymer concrete consists of sand, gravel, fly ash (FA), ground granulated blast furnace slag (GGBFS), NaOH(aq), and Na_2SiO_3(aq). Unlike previous mix design procedures [26], the specific gravity and volume of each ingredient and air content are considered. Accordingly, the GPC contains these components:

$$\text{GPC} = \text{sand} + \text{gravel} + \text{FA} + \text{GGBFS} + \text{NaOH(aq)} + \text{Na}_2\text{SiO}_3\text{(aq)} + \text{entrapped air} \quad (4)$$

An overall mix design procedure is demonstrated in Fig. 2. The procedure and calculations are explained in more detail below based on 1 L of GPC.

4.1. Preparation of alkaline solution

For most applications, the cost of the GPC should be taken into account. The alkaline solution is the most expensive GPC components (not considering the MPCMs). Based on previous studies [9], 200 g/L of alkaline solution was selected. Laboratory trials of workability and strength showed that 14 M NaOH (560 g/L) and a ratio of 1.5 between the Na_2SiO_3 solution and the NaOH solution was optimal. Accordingly, $m_{Na2SiO3(aq)}$ = 120 g, and $m_{NaOH(aq)}$ = 80 g, Where the Na_2SiO_3 solution contains 35 wt% Na_2SiO_3 (according to the manufacturer).

4.2. Liquid to geopolymer binder (L/GB)

It has been proposed that the ratio of the total mass of water (free water and water in the alkaline solution) to the total mass of geopolymer solids (FA, GGBFS, NaOH pellets and sodium silicate solid) is similar to the water to cement ratio (w/c) in Portland cement concrete [8,27]. However in this work, the total amount of liquid (L) is the sum of extra water, superplasticizer, and the entire alkaline solution (NaOH(aq) and $NaSiO_3$(aq)). The total amount geopolymer binder (GB) consists of FA and GGBFS [9]. In order to reach an adequate compressive strength for structural applications an initial L/GB ratio of 0.4 was chosen. However, in further steps extra water can be added to improve the workability of the mixture. After determination of the extra water content during the mixing process, this amount will be added to the initial liter of the mix design.

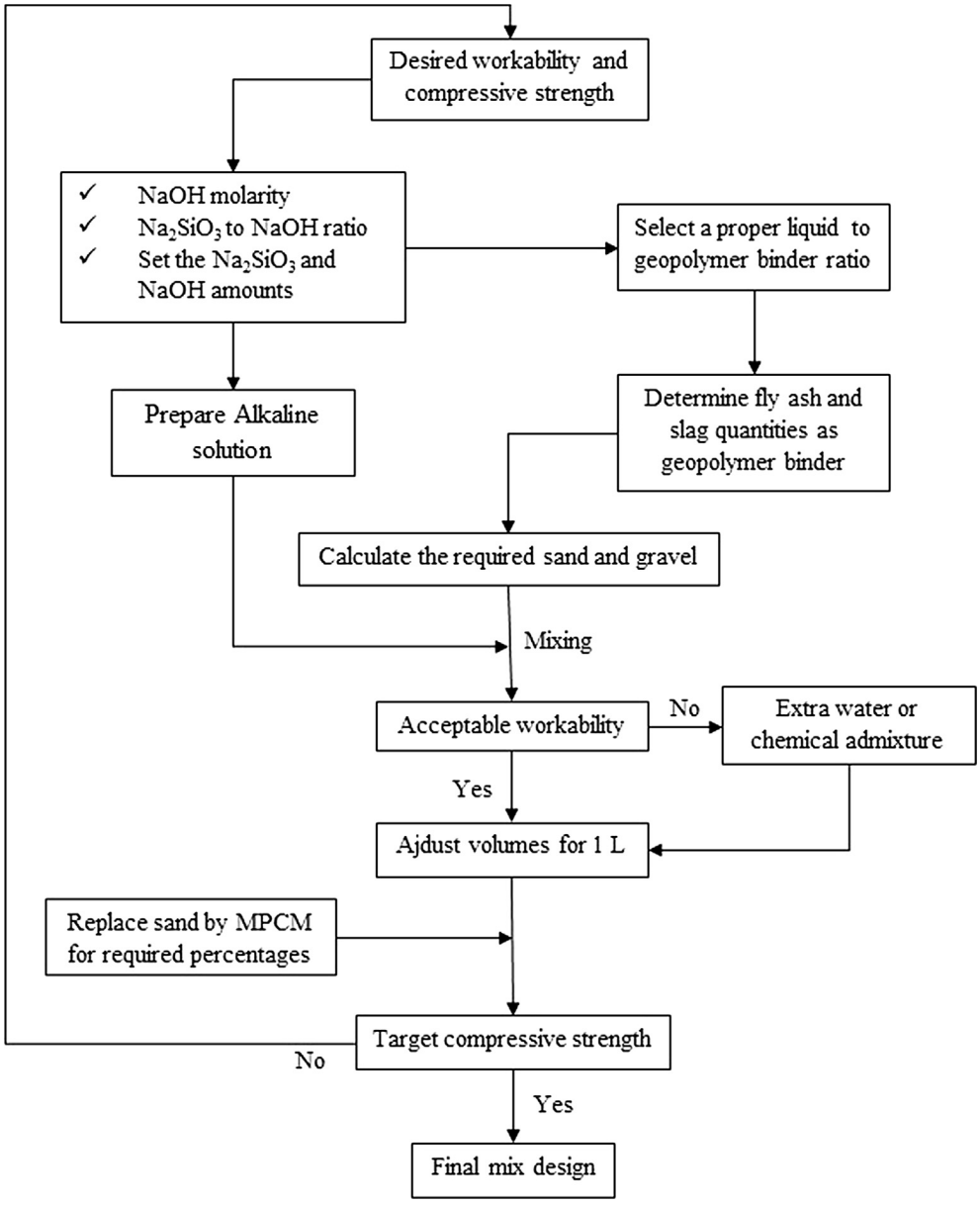

Fig. 2. The overall mix design procedure.

4.3. Determination of geopolymer binder (GB)

The addition of GGBFS to fly ash geopolymer concrete increases the compressive strength but reduces the workability and setting time [12]. Accordingly, an optimum mixture of FA and GGBFS can provide improved mechanical properties while keeping the workability and setting time within a usable range. Considering both workability and compressive strength after adding MPCM, a geopolymer binder (GB) consisting of 60% FA and 40% GGBFS was utilized. With an initial L/GB ratio of 0.4, and L = 200 g/L, we have GB = 500 g/L. Accordingly, for 1 L of sample, m_{FA} = 300 g, and m_{GGBFS} = 200 g.

4.4. Determination of required sand and gravel

FA, GGBFS, NaOH(aq), and Na_2SiO_3 are mixed at the determined amounts (total of 700 g/L, approximately 0.35 L for 1 L of GPC). Sand and gravel are added until the volume of the sample has the desired volume (1 L GPC). The total volume of sand and gravel in 1 L GPC is approximately 0.65 L. According to the particle size distribution, the volume percentages of sand and gravel are each considered to be 50% of the total volume of the sand and gravel mixture. Based on data sheets, the specific gravities of sand and gravel are 2680 and 2620 g/L, respectively. Accordingly, $m_{sand} \approx$ 871.18 g and $m_{gravel} \approx$ 851.68 g. The percentage of entrapped air in GPC has previously been found to be approximately 2% of the total volume [28].

4.5. Calculation of water and superplasticizing admixture

The first amount of water is equal to the total water in alkaline solution, i.e., 129.3 g, giving a water to geopolymer solid ratio of 0.23. The amounts of extra water and superplasticizer needed are obtained by experimental observation when mixing GPC without MPCMs. This step was repeated several times to gain the optimal amounts of extra water and superplasticizer, while keeping the workability and strength at acceptable levels. According to Nematollahi et al. [29], a superplasticizer amount corresponding to 1% of

Table 3
Amount of each ingredient per 1 L of Geopolymer concrete.

Ingredients	Volume (mL)	Amount (g)
NaOH solution	62	75.91
Na_2SiO_3 solution	59	113.87
Fly ash	124	280.24
GGBFS	67	190.95
Sand	309	828.12
Gravel	309	809.58
Extra water	47	47.00
Superplasticizer	4	4.80
Entrapped air	19	–
Total volume	1000	

the GB mass was chosen for the first step (5 g/L). The amount of extra water can be varied depending on the properties of the raw materials used. In this study, 50 g extra water was found to be optimal.

4.6. Adjustment of proposed mix design for 1 L

After adding extra water and superplasticizer to obtain an improved mixture, the total volume of the original 1 L mix increases to 1.05 L. To obtain a 1 L mix design recipe again, the amount of each component is simply divided by 1.05. After these adjustments, the mixture design for 1 L GPC containing 0% MPCM is shown in table 3.

4.7. Calculation of MPCMs replacement

There are two methods to add MPCMs to GPC which are called the MPCM replacement method and the MPCM additive method. Pania et al. [30] observed that the strength reduction of concrete was less when the MPCM replaced a certain percentage of sand (MPCM replacement method) than when the MPCM was added to the concrete mixture as an extra additive (MPCM additive method). Based on the MPCM replacement method, different MPCM percentages (in volume) are replaced with the same percentages of sand. In this study, 0, 10 and 20% of sand are replaced by two different MPCMs with densities of 900 g/L. The summary of the amounts of sand replaced by MPCM is given in Table 4:

4.8. Mixing method

The alkaline solution was prepared 1 day in advance to ensure complete dissolution of NaOH pellets and to lose the exothermic reaction heat. During storage, the NaOH solution was hermetically closed to avoid carbonation. For the setting time measurements, the alkaline solution and geopolymer binder with a ratio of 0.4 were mixed together for 90 s, according to the EN 196-3 recommendations. Afterward the MPCM was introduced to the paste and mixed for another 90 s into a homogenous combination. Due to the absence of sand, MPCM was added by the additive method.

For GPC preparation, the paste (without MPCM) was introduced into the dried sand and mixed for 30 s. Subsequently, gravel was added to the mixture and mixed for 2 min. During these 2 min mixing, superplasticizer and extra water were added to the mixture separately. Afterwards, the MPCM was added to the mixture and mixing was continued for 2 more minutes. The MPCM was added as the last component in order to limit the damage to the MPCM shell during the mixing process [30].

4.9. Casting and curing

The GPC samples with 0, 10, and 20 vol% of the sand replaced by PE-EVA-PCM or St-DVB-PCM, were cast according to the procedure described previously in [7] at 20 °C. After casting, the specimens were pre-cured at ambient temperature with a relatively humidity of 90% for 24 h. After demolding, the samples were cured in water at 20 °C for 1, 7, 14, and 28 days.

Table 4
Amount of sand replacement by MPCM.

	MPCM (vol%)	Sand (g)	MPCM (g)
GPC0	0	828.12	0
GPC10	10	745.31	27.9
GPC20	20	662.49	55.8

5. Results and discussion

5.1. Particle size distribution and water content

The particle size distributions of sand, gravel, PE-EVA-PCM, St-DVB-PCM, fly ash, and ground granulated blast furnace slag are displayed in Fig. 3. Both types of microcapsules are smaller than the replaced sand. As can be seen in Fig. 1a, PE-EVA-PCM has a strong tendency to form large agglomerated structures (D60 = 240 μm) [6,7], which is probably the main reason for the presence of larger particles in this sample. It should be noted that the uneven shapes of PE-EVA-PCM and its agglomerates might affect the apparent sizes displayed in Fig. 3, as the calculations are based on spherical particles.

The water adsorbed and retained by PE-EVA-PCM, St-DVB-PCM and sand after immersion in water is shown in Fig. 4. The amount of water contained by the samples after immersion is related to how much water the particles retain in the geopolymer mixture. It is clear from Fig. 4a that the MPCMs adsorb more water than sand per unit mass. This is probably due to the smaller sizes of the microcapsules (Fig. 3), which results in a larger total surface area. Although the sizes of the microcapsules are similar, PE-EVA-PCM adsorbs more water than St-DVB-PCM. This is in agreement with the more hydrophobic nature of the St-DVB shell, compared to PE-EVA which contains some polar groups. Since the MPCM replaces sand by volume in the geopolymer matrix, the water adsorption per volume unit of dry material is displayed in Fig. 4b. The microcapsules also adsorb more water than sand when

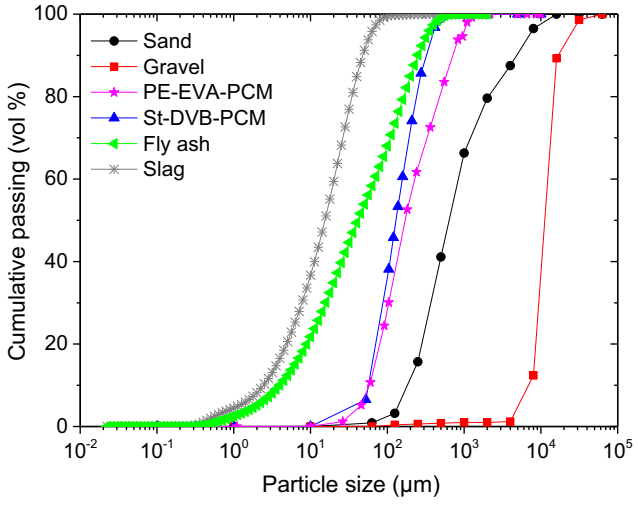

Fig. 3. Particle size distributions of sand, gravel, PE-EVA-PCM, St-DVB-PCM, fly ash, and ground granulated blast furnace slag.

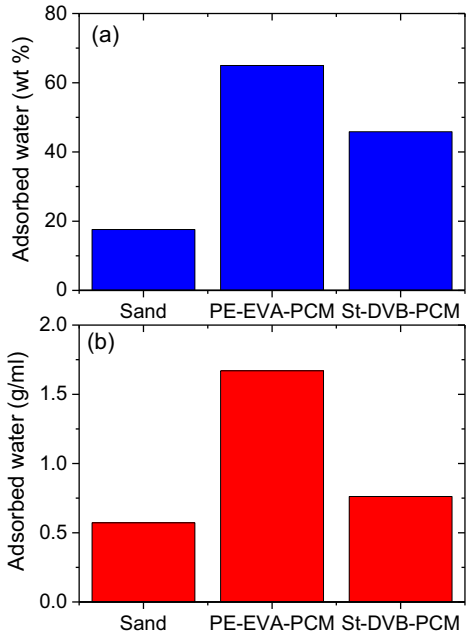

Fig. 4. (a) Weight percentage of adsorbed water of sand, PE-EVA-PCM, and St-DVB-PCM after immersion in water, and (b) adsorbed water per volume unit of sand, PE-EVA-PCM, and St-DVB-PCM.

volumes are considered instead of weights. However, the difference between sand and St-DVB-PCM is less evident and the difference between the two types of microcapsules is much more obvious. Accordingly, the polarity of the microcapsule shell is more important for how much water the samples adsorb than the differences in sizes, although the latter also has a clear effect on the water adsorption.

5.2. Slump flow test

In order to verify the quality of the mix design after the addition of MPCMs, the workability was carried out by a slump test. As can be seen from Fig. 5, there is a decrease in the workability (lower slump) of fresh GPC after adding MPCM. This can be explained by the higher amount of water adsorbed by the microcapsules compared to the MPCM replaces (Fig. 4). This causes a reduction of the flowability of GPC, in agreement with previous findings [7,19]. Due to the higher water adsorption (Fig. 4b), the addition of PE-EVA-PCM causes a much steeper decline of the slump (slope = −4) than St-DVB-PCM (slope = −0.5).

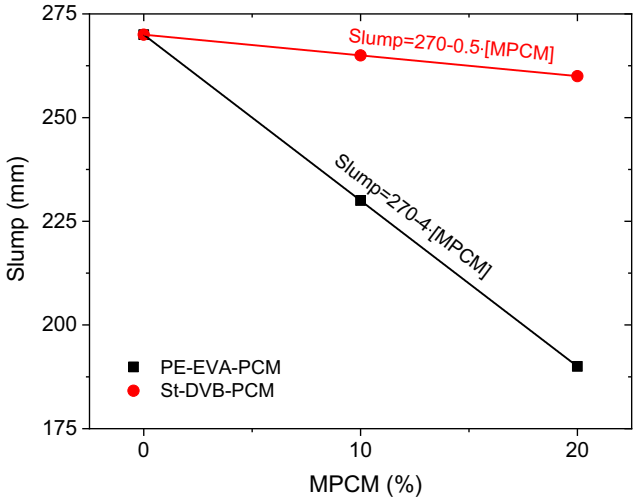

Fig. 5. Slump of GPC containing various amounts of PE-EVA-PCM and St-DVB-PCM.

5.3. Setting time

Fig. 6a shows the effect of MPCM addition on the initial and final setting times of geopolymer paste. Increasing the MPCM concentration slightly delays the initial setting time, but causes a significantly faster final setting time in comparison to geopolymer paste without MPCM. As illustrated in the inset plot of Fig. 6b, reducing the amount of available water decreases both the initial and final setting times. This can explain why the final setting time becomes shorter when MPCM is added to the samples. However, a larger difference between the two types of MPCM should be expected, since PE-EVA-PCM adsorbs much more water than St-DVB-PCM (Fig. 4b).

The geopolymer reaction rates can be slowed down when the viscosity of the samples increases [17,31,32]. This can help to explain the longer initial setting times in the presence of MPCM. Since PE-EVA-PCM has a much stronger effect on the slump than St-DVB-PCM (Fig. 5), the effect of viscosity on the reaction rates is expected to be larger in the presence of PE-EVA-PCM. In addition, the latent heat of the microcapsules may slow down the setting times by absorbing reaction heat (preventing the samples from becoming warmer, which would speed up the reaction rate). This effect would probably be similar for the two types of MPCM, since their latent heat are practically the same (Table 2).

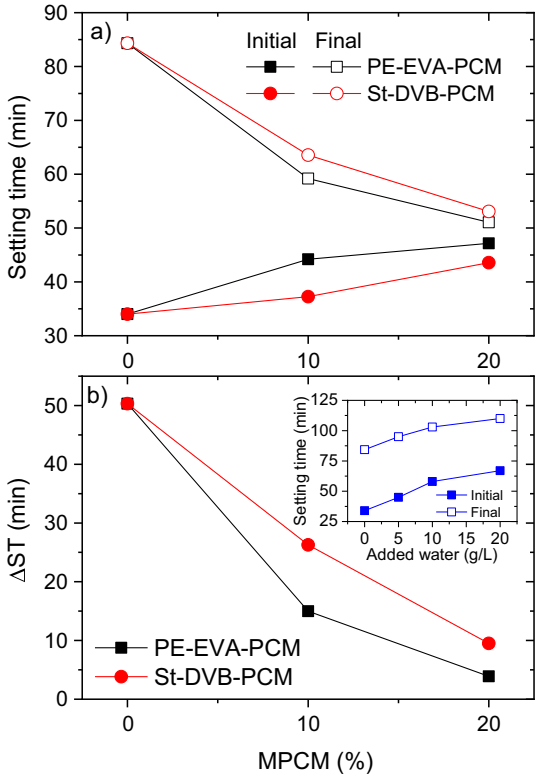

Fig. 6. a) The initial and final setting times of geopolymer paste containing various amounts of PE-EVA-PCM and St-DVB-PCM. b) The difference between the initial and final setting times (ΔST). The inset plot illustrates the effect of added water on the setting times of the samples.

Accordingly, when microcapsules are added to the geopolymer paste, the reduced amount of available water (Fig. 4b) shortens the initial setting time while the increased viscosities (lower slump, Fig. 5) and latent heat slow down the reaction rates. The initial setting times (Fig. 6a) are a result of these competing mechanisms. The increase of the initial setting times illustrates that the viscosity and/or latent heat are the dominating effects at this stage. Since both the viscosity increase and the water adsorption are strongest for EP-EVA-PCM, there is only a moderate difference in initial setting time between the two types of MPCM.

When the initial setting time is reached, the samples have started to solidify, and the effect of viscosity on further reactions is negligible for all samples. The release of reaction heat is strongest at short times, and the effect of the MPCM latent heat is probably small when the initial setting time is approached. Accordingly, at this stage the water content is the determining factor. Fig. 6b shows the time between the initial and final setting times (ΔST). As expected, ΔST decreases with the concentration of MPCM due to the adsorption of water onto the surface of the microcapsules. This effect is strongest for PE-EVA-PCM, which has a higher water adsorption (Fig. 4b).

The final setting times are a combination of the initial setting time and ΔST. Since the water content influences the whole process while the viscosity and latent heat only affects the initial stage, the overall effect on the final setting time is dominated by the water content. Accordingly, the final setting time becomes shorter in the presence of MPCM. The dominating effect at each stage has a larger impact on PE-EVA-PCM than on St-DVB-PCM. As a result, the initial setting times are longer and the final setting times shorter for PE-EVA-PCM.

5.4. Compressive strength

Fig. 7 shows the compressive strength of the GPC mixture with incorporated PE-EVA-PCM and St-DVB-PCM after 1, 7, 14, and 28 days curing at 20 °C. The maximum compressive strength of Portland cement concrete after 28 days curing at ambient temperature according to [33] is also shown for comparison. The water to cement ratio of this Portland cement concrete is 0.5 which is equal to the L/GB ratio in the current proposed mix design.

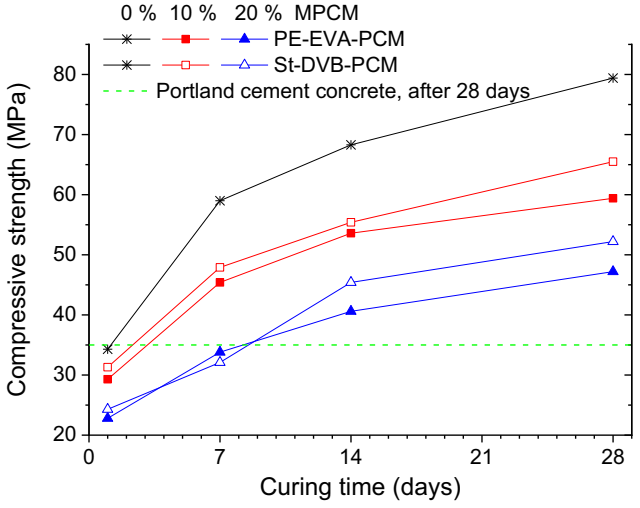

Fig. 7. Compressive strength of GPC (cured at 20 °C) versus curing time when 0, 10, and 20% sand is replaced by PE-EVA-PCM or St-DVB-PCM. The green dashed line illustrates the maximum compressive strength of PCC after 28 days curing at ambient temperature [33]. (For interpretation of the references to color in this figure legend, the reader is referred to the web version of this article.)

As expected, the compressive strength of the proposed GPC mixture increases with curing time. In order to evaluate whether the proposed GPC mix design with incorporated MPCMs is suitable for structural purposes, the maximum compressive strength of Portland cement concrete after 28 days [33] is shown for comparison. The first day strength of the proposed GPC without PCM is almost the same as for Portland cement concrete after 28 days (around 35 MPa). In spite of the negative effect of both PE-EVA-PCM and St-DVB-PCM on the strength of GPC, the compressive strength of GPC with 20% MPCMs after 28 days curing is significantly higher than for Portland cement concrete. Utilizing a GGBFS in addition to fly ash contributes to this good mechanical strength [12].

Fig. 7 also illustrates the effect of different types of MPCM on the mechanical properties of GPC. The strength of GPC containing MPCM is lower than GPC without MPCM, which is in agreement with previous findings [7,10,34]. This reduction of the mechanical properties is probably a combination of several effects. The sand is replaced by MPCM, which reduces the compressive strength due to a lower compactness and stiffness of the microcapsules compared to sand [8]. In addition, utilizing MPCM causes more air voids to be formed in the concrete matrix, which have a negative impact on the mechanical strength [6,34]. A poorer dispersion of small particles in the concrete can also have a negative effect on the compressive strength [35,36], and air gaps between MPCM and the concrete matrix may reduce the compressive strength [7,34].

The irregular shell of PE-EVA-PCM and its tendency to form agglomerates can contribute to the larger strength reduction of GPC containing with PE-EVA-PCM compared to St-DVB-PCM. In addition, the lower workability of PE-EVA-PCM (Fig. 5) might contribute to more air being trapped in these samples, thereby reducing the compressive strength. To further investigate how MPCM are affecting the microstructure of GPC, SEM analysis and X-ray micro-tomography have been conducted.

5.5. Microstructural analysis

The failure surface of GPC samples with 20% PE-EVA-PCM and St-DVB-PCM were selected for SEM analyses. Fig. 8 presents an individual particle of PE-EVA-PCM and St-DVB-PCM in the matrix as an example of MPCM diameters and the gap observed in the shell-concrete matrix transition zone. As can be seen from Fig. 8, there are smaller gaps between St-DVB-PCM and the GPC matrix than for PE-EVA-PCM. This might contribute to the lower compressive strength of GPC containing PE-EVA-PCM (Fig. 7). However, it should be noted that one microcapsule and its surrounded matrix may not be representative of the whole sample.

Fig. 9 a and b show how the MPCMs are distributed in the concrete matrix. For St-DVB-PCM every particle is visible while for PE-EVA-PCM, large agglomerates are observed. Fig. 9c and d show the single microcapsules after the compressive strength test (at the failure surface of the GPC). The shell of the microcapsules can be broken during the compressive strength measurements, which might be a contributing factor to the reduced compressive strength (Fig. 7). This is illustrated in Fig. 9d, where the St-DVB-PCM capsule is clearly broken. Unfortunately, due to the irregular shell of PE-EVA-PCM, a broken shell cannot be easily distinguished from an undamaged shell. However, the line indicated by the arrow in Fig. 9c might be a rupture on the PE-EVA-PCM shell.

Typical 2D X-ray micro-tomography cross-sectional slices obtained from GPC, without and with 20% PE-EVA-PCM and St-DVB-PCM, are shown in Fig. 10. Due to the low X-ray attenuation of organic materials it is difficult to distinguish the microcapsules from air voids based on grey scale values. PE-EVA-PCM has an irregular shape (Fig. 1a) which makes it possible to distinguish them from the spherical air voids. However, it is difficult to distinguish the nearly spherical St-DVB-PCM (Fig. 1b) from the air voids.

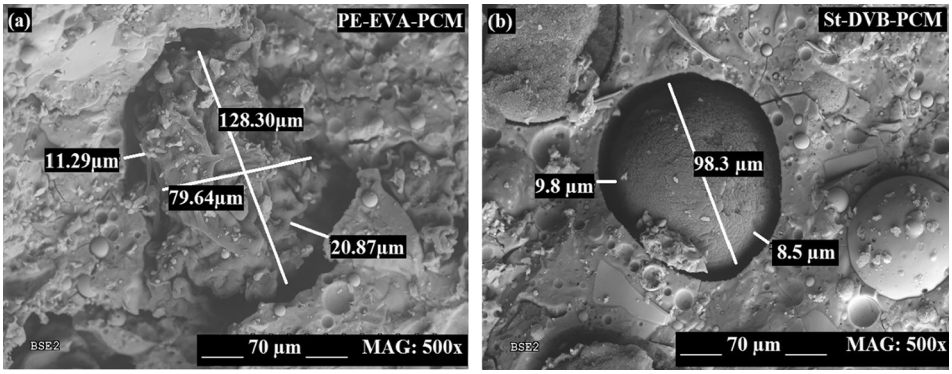

Fig. 8. SEM images of the fracture surface of GPC with incorporated 20% (a) PE-EVA-PCM, (b) St-DVB-PCM.

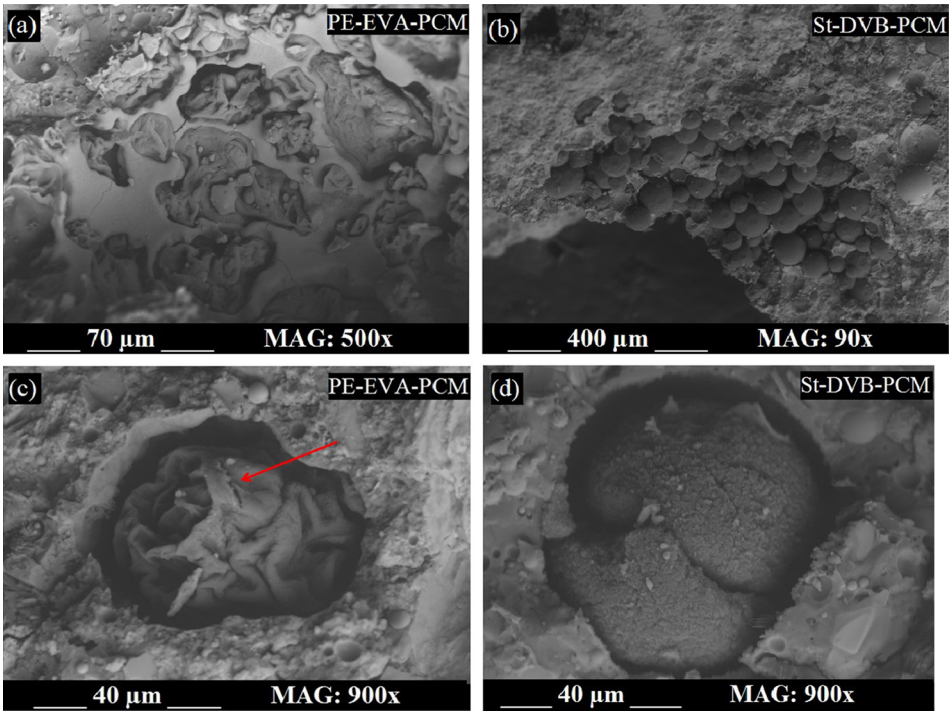

Fig. 9. SEM images of the GPC matrix including agglomeration of (a) PE-EVA-PCM, (b) St-DVB-PCM, (c) shell of PE-EVA-PCM the arrow shows a possible rupture of the shell, and (d) damaged shell of St-DVB-PCM.

The large and relatively homogenous areas in Fig. 10 are the gravel, which is surrounded by the GPC matrix where the MPCM and air voids are evident as black spots. Comparing the non-gravel parts of the concrete matrix, PE-EVA-PCM seems to be riddled with more black areas than St-DVB-PCM, suggesting that PE-EVA-PCM contains more air voids. This is probably a contributing factor to the lower compressive strength of PE-EVA-PCM (Fig. 7). The higher amounts of air voids might be due to the poorer workability (Fig. 5), which can cause air to be trapped within the concrete matrix.

3D volume rendering of GPC with PE-EVA-PCM and St-DVB-PCM are displayed in Fig. 11. The irregular agglomerates of PE-EVA-PCM are also evident in Fig. 11a. As discussed above, the presence of large agglomerates and a lower stiffness of the microcapsules might influence the properties of GPC.

Size distributions based on image analysis of the 3D X-ray-tomography are shown in Fig. 12. As discussed above, it is difficult to distinguish the microcapsules and the air voids from each other, and accordingly the size distributions in Fig. 12 are a combination of microcapsules and air. There are no significant differences between the two samples. The size distributions of the pure microcapsules are added to Fig. 12b to show the absolute contribution of MPCM to the total porosity computed by µ-CT. Interestingly, the sizes measured inside the GPC matrix are much smaller than the pure microcapsules. This might be due to a disruption of agglomerates into smaller entities (caused by shear forces during the mixing process), or that the volume fractions are dominated by small air voids.

5.6. Energy saving

The power reduction during a 24 h period of GPC containing 20% MPCM compared to GPC without PCM is displayed in Fig. 13. PE-EVA-PCM seems to be able to save slightly more energy than St-DVB-PCM. Since the PCM content are the same and the latent heat of the microcapsules are very similar (Table 2), the differences in saved energy is probably due to a higher amount of air voids in the GPC containing PE-EVA-PCM. Air is a very poor conductor of heat, and accordingly air voids will induce an insulating effect.

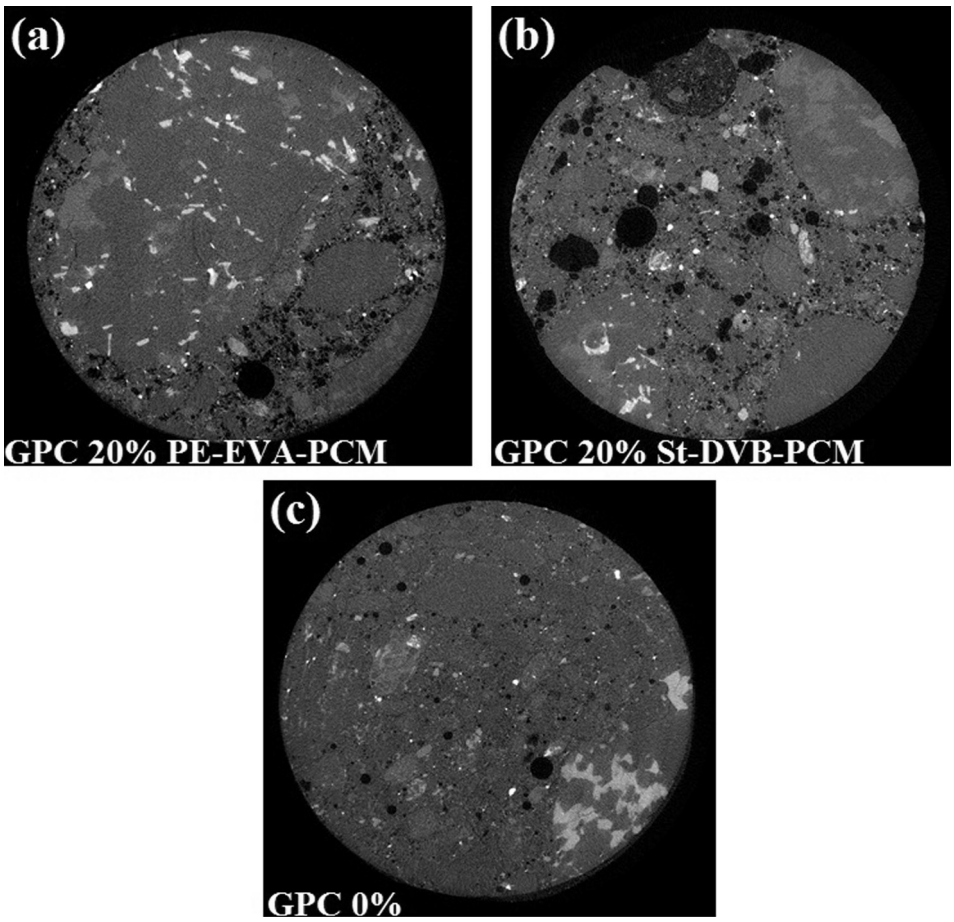

Fig. 10. X-ray-tomography images of (a) GPC with 20% PE-EVA-PCM, (b) GPC with 20% St-DVB-PCM and (c) GPC without MPCM. Dark colors correspond to low or no absorption of X-rays (e.g. air bubbles or microcapsules) and bright colors represent high absorption of X-rays (sand and gravel). The field of view is approximately 1 cm.

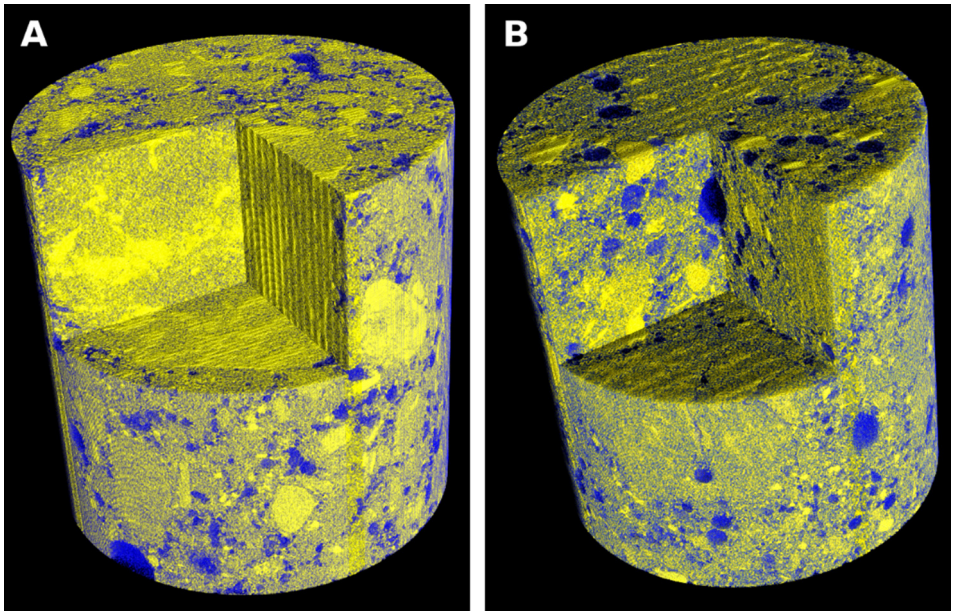

Fig. 11. False-color 3D volume rendering of GPC cylindrical drill cores including A: PE-EVA-PCM, B: St-DVB-PCM. The MPCMs and air voids are displayed in blue. (For interpretation of the references to color in this figure legend, the reader is referred to the web version of this article.)

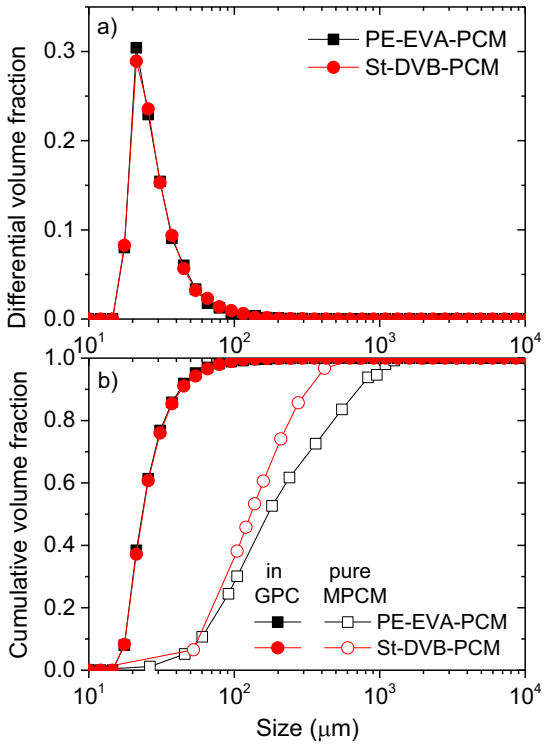

Fig. 12. Differential (a) and cumulative (b) size distributions of MPCM and air voids inside the GPC samples, obtained from image analyses of the X-ray-tomography images. The cumulative size distributions of the pure microcapsules are shown for comparison.

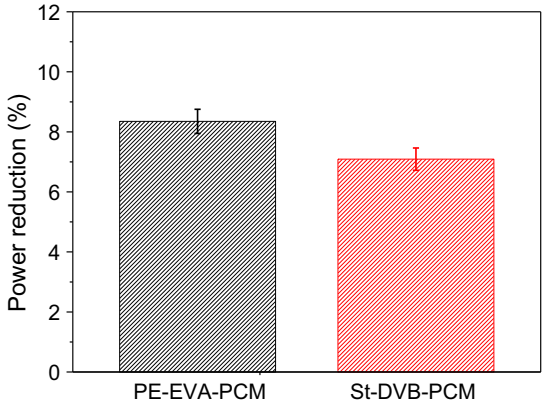

Fig. 13. The power reduction of GPC containing 20% MPCM compared to a corresponding sample without MPCM during a 24 h period with an outdoor temperature variation between 10 and 40 °C, and an indoor temperature of 23 °C.

6. Conclusions

A reliable mix design procedure for class F fly ash/slag GPC has been developed to achieve high compressive strength after the addition of MPCM. To validate the mix design and the effect of two different types of MPCM, water absorption of the raw materials, setting time, slump test and compressive strength determination were carried out. The main findings of this study are:

- The percentage of absorbed and retained water of the MPCMs is higher than for sand. More water is adsorbed onto PE-EVA-PCM than for St-DVB-PCM due to the polar groups of the PE-EVA-PCM shell.
- Increasing the amount of MPCM reduced the workability of both PE-EVA-PCM and St-DVB-PCM. The higher water adsorption PE-EVA-PCM caused a lower slump of GPC containing PE-EVA-PCM than for St-DVB-PCM.
- The initial setting time of geopolymer paste increased with the addition of MPCM, while the final setting time became shorter. There are several competing factors affecting the setting time. The adsorbed water reduces the setting time while the setting time is raised by a slower reaction rate caused by the increased viscosity of the samples and possibly by the latent heat of the MPCM, which can prevent a temperature rise from the reaction heat.
- The compressive strength is lower in the presence of PE-EVA-PCM. The agglomerated and non-spherical structure of PE-EVA-PCM and a higher amount of air voids might contribute to the reduced workability and lower compressive strength.
- The proposed mix design could successfully overcome the strength reduction after adding MPCM. After 28 days, the compressive strength of GPC including 20% MPCM (replacing sand) was higher than for Portland cement concrete without MPCM. Accordingly, in spite of the negative effect of the MPCMs on the properties of GPC, the compressive strength is still sufficiently high for structural applications (acceptable range of compressive strength is between 25 and 40 MPa).
- Microstructural studies reveal smaller gaps between St-DVB-PCM and the GPC matrix than for PE-EVA-PCM.
- MPCM agglomeration and MPCM capsules that are broken during the compressive strength test are probably contributing to the strength reduction after adding MPCM to GPC.
- PE-EVA-PCM exhibits a somewhat better energy saving potential than St-DVB-PCM, which is probably due to a higher content of insulating air voids.

Conflict of interest

The authors declare that we have no conflict of interest with respect to this paper.

Acknowledgements

This work was supported by the Research Council of Norway, grant number 238198. The authors acknowledge the Ministerio de Economía, Industria y Competitividad (MINECO, Spain), the EU FEDER Program (Grant # MAT2017-85130-P).

References

[1] D.J.M. Flower, J.G. Sanjayan, Green house gas emissions due to concrete manufacture, Int. J. Life Cycle Assess. 12 (2007) 282.
[2] M. Schneider, M. Romer, M. Tschudin, H. Bolio, Sustainable cement production—present and future, Cem. Concr. Res. 41 (2011) 642–650.
[3] J. Davidovits, Geopolymer Chemistry and Applications, Institute Géopolymère, Saint-Quentin, France, 2011.
[4] W.K. Part, M. Ramli, C.B. Cheah, An overview on the influence of various factors on the properties of geopolymer concrete derived from industrial by-products, Constr. Build. Mater. 77 (2015) 370–395.
[5] D. Hardjito, S.E. Wallah, D.M. Sumajouw, B.V. Rangan, On the development of fly ash-based geopolymer concrete, ACI Mater. J. Am. Conc. Inst. 101 (2004) 467–472.
[6] V.D. Cao, S. Pilehvar, C. Salas-Bringas, A.M. Szczotok, J.F. Rodriguez, M. Carmona, N. Al-Manasir, A.-L. Kjøniksen, Microencapsulated phase change materials for enhancing the thermal performance of Portland cement concrete and geopolymer concrete for passive building applications, Energy Convers. Manage. 133 (2017) 56–66.
[7] S. Pilehvar, V.D. Cao, A.M. Szczotok, L. Valentini, D. Salvioni, M. Magistri, R. Pamies, A.-L. Kjøniksen, Mechanical properties and microscale changes of geopolymer concrete and Portland cement concrete containing micro-encapsulated phase change materials, Cem. Concr. Res. 100 (2017) 341–349.
[8] M. Talha Junaid, O. Kayali, A. Khennane, J. Black, A mix design procedure for low calcium alkali activated fly ash-based concretes, Constr. Build. Mater. 79 (2015) 301–310.

[9] P. Pavithra, M.S. Reddy, P. Dinakar, B.H. Rao, B. Satpathy, A. Mohanty, A mix design procedure for geopolymer concrete with fly ash, J. Cleaner Prod. 133 (2016) 117–125.
[10] R. Shadnia, L. Zhang, P. Li, Experimental study of geopolymer mortar with incorporated PCM, Constr. Build. Mater. 84 (2015) 95–102.
[11] E.I. Diaz, E.N. Allouche, S. Eklund, Factors affecting the suitability of fly ash as source material for geopolymers, Fuel 89 (2010) 992–996.
[12] P. Nath, P.K. Sarker, Effect of GGBFS on setting, workability and early strength properties of fly ash geopolymer concrete cured in ambient condition, Constr. Build. Mater. 66 (2014) 163–171.
[13] A.M. Rashad, A comprehensive overview about the influence of different admixtures and additives on the properties of alkali-activated fly ash, Mater. Des. 53 (2014) 1005–1025.
[14] S. Kumar, R. Kumar, S.P. Mehrotra, Influence of granulated blast furnace slag on the reaction, structure and properties of fly ash based geopolymer, J. Mater. Sci. 45 (2010) 607–615.
[15] T. Phoo-ngernkham, A. Maegawa, N. Mishima, S. Hatanaka, P. Chindaprasirt, Effects of sodium hydroxide and sodium silicate solutions on compressive and shear bond strengths of FA–GBFS geopolymer, Constr. Build. Mater. 91 (2015) 1–8.
[16] D. Panias, I.P. Giannopoulou, T. Perraki, Effect of synthesis parameters on the mechanical properties of fly ash-based geopolymers, Colloids Surf., A 301 (2007) 246–254.
[17] U. Rattanasak, P. Chindaprasirt, Influence of NaOH solution on the synthesis of fly ash geopolymer, Miner. Eng. 22 (2009) 1073–1078.
[18] A.A. Aliabdo, A.E.M. Abd Elmoaty, H.A. Salem, Effect of water addition, plasticizer and alkaline solution constitution on fly ash based geopolymer concrete performance, Constr. Build. Mater. 121 (2016) 694–703.
[19] S.-K. Park, J.-H.J. Kim, J.-W. Nam, H.D. Phan, J.-K. Kim, Development of anti-fungal mortar and concrete using Zeolite and Zeocarbon microcapsules, Cem. Concr. Compos. 31 (2009) 447–453.
[20] J. Xie, O. Kayali, Effect of superplasticiser on workability enhancement of Class F and Class C fly ash-based geopolymers, Constr. Build. Mater. 122 (2016) 36–42.
[21] A.M. Borreguero, J.L. Valverde, J.F. Rodríguez, A.H. Barber, J.J. Cubillo, M. Carmona, Synthesis and characterization of microcapsules containing Rubitherm®RT27 obtained by spray drying, Chem. Eng. J. 166 (2011) 384–390.
[22] A.M. Szczotok, M. Carmona, A.-L. Kjøniksen, J.F. Rodriguez, Equilibrium adsorption of polyvinylpyrrolidone and its role on thermoregulating microcapsules synthesis process, Colloid Polym. Sci. 295 (2017) 783–792.
[23] L. Feldkamp, L. Davis, J. Kress, Practical cone-beam algorithm, JOSA A 1 (1984) 612–619.
[24] S.C.T.W. Ridler, Picture thresholding using an iterative selection method, IEEE Trans. Syst. Man Cybern. 8 (1978).
[25] V.D. Cao, S. Pilehvar, C. Salas-Bringas, A.M. Szczotok, T.Q. Bui, M. Carmona, J.F. Rodriguez, A.-L. Kjøniksen, Thermal performance and numerical simulation of geopolymer concrete containing different types of thermoregulating materials for passive building applications, Submitted for publication, (2018).
[26] N. Lloyd, V. Rangan, Geopolymer concrete with fly ash, Proceedings of the Second International Conference on Sustainable Construction Materials and Technologies, UWM Center for By-Products Utilization, 2010, pp. 1493–1504.
[27] W. Ferdous, A. Manalo, A. Khennane, O. Kayali, Geopolymer concrete-filled pultruded composite beams – concrete mix design and application, Cem. Concr. Compos. 58 (2015) 1–13.
[28] R. Anuradha, V. Sreevidya, R. Venkatasubramani, B.V. Rangan, Modified guidelines for geopolymer concrete mix design using Indian standard, Asian J. Civil Eng. (Building and Housing) 13 (2012) 353–364.
[29] B. Nematollahi, J. Sanjayan, Effect of different superplasticizers and activator combinations on workability and strength of fly ash based geopolymer, Mater. Des. 57 (2014) 667–672.
[30] M. Pania, X. Yunping, Effect of phase-change materials on properties of concrete, Mater. J. (2012) 109.
[31] P. Sashi, A.K. Bhuyan, Viscosity dependence of some protein and enzyme reaction rates: seventy-five years after Kramers, Biochemistry 54 (2015) 4453–4461.
[32] A. Kumar, S.S. Pawar, High viscosity of ionic liquids causes rate retardation of Diels-Alder reactions, Sci. China-Chem. 55 (2012) 1633–1637.
[33] S.H. Kosmatka, B. Kerkhoff, W.C. Panarese, N.F. MacLeod, R.J. McGrath, Design and Control of Concrete Mixtures, Seventh Canadian Edition, Cement Association of Canada, 2002, p. 151.
[34] M. Hunger, A. Entrop, I. Mandilaras, H. Brouwers, M. Founti, The behavior of self-compacting concrete containing micro-encapsulated phase change materials, Cem. Concr. Compos. 31 (2009) 731–743.
[35] F. Vahedi, H.R. Shahverdi, M.M. Shokrieh, M. Esmkhani, Effects of carbon nanotube content on the mechanical and electrical properties of epoxy-based composites, New Carbon Mater. 29 (2014) 419–425.
[36] H. Elkady, M.I. Serag, M.S. Elfeky, Effect of Nano Silica De-agglomeration, and Methods of Adding Super-plasticizer on the Compressive Strength, and Workability of Nano Silica Concrete, Civil Environ. Res. 3 (2013) 21–34.